Recent Res. Devel. Quantum Electronics, 1 (1999):137-164

Time-dependent phenomena in unintentionally disordered superlattices

F. Domínguez-Adame, E. Diez* and J. Devís*
GISC, Departamento de Física de Materiales, Universidad Complutense, E-20840 Madrid, Spain; *GISC, Departamento de Matemáticas, Universidad Carlos III, E-28911 Leganés, Madrid, Spain

Recent advances in laser technology make it possible to drive semiconductor superlattices with intense ac-dc fields, opening the possibility to study new effects that depend in a crucial way on the spatio–temporal coherence of electronic states. Coherent oscillations in semiconductor superlattices present finite lifetime and tend to disappear. This article gives a brief review of the effects of unintentional disorder appearing during growth on coherent phenomena in semiconductor superlattices, aiming to highlight the relevance of unintentional disorder in coherent transport phenomena as a dephasing mechanism.

1. INTRODUCTION

The starting point of the history of semiconductor superlattices (SLs) was a short paper by Leo Esaki and Ray Tsu, appeared in the IBM Journal of Research and Development in 1970 [1]. Three decades after, semiconductor heterostructures represent about 50% of the efforts in semiconductor physics worldwide. In their seminal paper, the authors speculated that a periodic modulation of the composition or doping of a semiconductor at a length scale smaller than the electron mean free path would result in the occurrence of minibands, showing strong energy dispersion effects and leading to negative differential conductance mechanisms.

Earlier attempts to growth high-quality SLs used the chemical vapor deposition technique in GaAs-$GaAs_{1-x}P_x$ materials system [2]. The relatively large lattice-constant mismatch caused difficulties and results were somewhat disappointing. Subsenquenly, researchers devoted their attention to GaAs-$Ga_{1-x}Al_xAs$ materials system since the lattice-constant mismatch is rather small — less than 0.1%— in this case [3,4]. Quantum confinement was demonstrated through the observation of negative differential resistance in SLs [5]. It was then realized that new phys-

ical effects might occur in SLs, thus opening the possibility to growth synthetic materials with the desired electrical and optical properties. Technological advances in semiconductor microfabrication based on molecular-beam epitaxy, pioneered in the late 1960s by Chao and Arthur at AT&T Bell Laboratories, now makes it possible to growth ultrathin layers, on the order of few atomic monolayers, with sharp interfaces. Moreover, SLs are not restricted to GaAs-$Ga_{1-x}Al_xAs$ materials system but other III-V and II-VI compound semiconductors are used in nanoelectronic modeling. However, since GaAs-$Ga_{1-x}Al_xAs$ heterojunctions are by far the most throughly investigated system, we will mainly focus our attention on type I SLs, where electrons and holes are confined in the same semiconductor layer.

Theory of ideal SLs electronic structure and optical properties is based on solid grounds. There already exist a number of reviews [6] and text books [7] dealing with electronic structure of SLs with different energy-band lineups, strain conditions, growth orientations and applied electromagnetic fields. In most cases of interest, the envelope-function method (EFM) within the one-band approximation provides a reasonable description of the electronic states near the zone-center of type I SLs made of wide gap semiconductors [8]. This approach assumes that the electron wave function is the product of a zone-center Bloch function and a slowly varying envelope-function. Bloch functions of III-V compounds are very similar close to the zone-center so that each semiconductor layer is characterized only by the effective mass of electrons and holes, whereas the heterojunction is usually modeled as a step-like potential whose height is given by the conduction- or valence-band offset.

Figure 1 shows the spatial modulation of both conduction- and valence-band edges at the Γ valley of a generic type I SL — *canonical* example is GaAs-$Ga_{1-x}Al_xAs$—, where GaAs acts as a potential well for both electrons and holes. The effective mass and the band offset at GaAs-$Ga_{1-x}Al_xAs$ interfaces depend on the Al fraction. They are given by $m^*/m_0 = 0.067 + 0.083x$ (here m_0 denotes the free electron mass) and $\Delta E_c = 1.1x$ eV for $0 \leq x \leq 0.45$ [9].

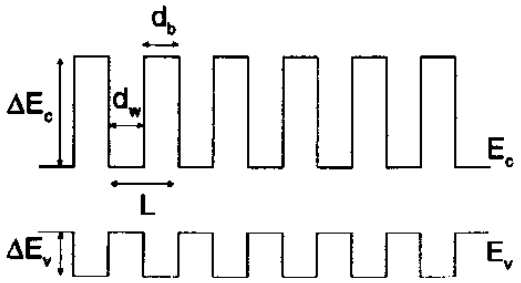

FIG. 1. Conduction-band and valence-band edges profiles in type I SLs.

In spite of the recent advances in semiconductor growth techniques [10,11], the fabrication of abrupt interfaces with perfect atomic arrangement cannot be achieved and some amount of disorder is unavoidable. With the structural characterization techniques now available, it has become apparent that not only semiconductor interfaces are almost never ideal, but that the occurrence of *unintentional* disorder due to growth imperfections has profound effects on spectroscopy [12–14] and transport properties [15–17] of semiconductor structures.

Possible conflicts between experiments and theoretical models based on the assumption

of abrupt interfaces are often settled by adjusting fitting parameters (effective mass and band offset). However, this approach cannot explain the rich phenomenology of disordered heterostructures, like electron localization at imperfect interfaces [18]. More general models including unintentional disorder would then be more adequate for studying electron dynamics in actual SLs. In this paper we review recent theoretical efforts toward this goal. We will be concerned ourselves with time-dependent envelope function method in unintentionally disordered SLs subjected to dc and ac applied fields.

The review is organized as follows. In Section 2 we describe the model devised to take into account the effects of nonideal interfaces on electron dynamics. We will discuss in some detail the approaches commonly used to include randomness in the effective-mass theory while keeping the model as simple as possible. Section 3 deals with imperfect SLs in the absence of external fields; in particular, we will discuss the steady state regime and also wave packet dynamics. In Section 4 we will review the so called Bloch oscillations and dynamical localization, observed in SLs under dc applied electric fields. As main point, we claim that disorder plays a major role in the decay of coherent oscillations. Electron dynamics in SLs subject to ac fields due to strong high-frequency laser is studied in Section 5. We will point out that Rabi oscillations between minibands could be detected in SLs under ac fields, in close analogy with two-level atoms. Section 6 presents a nonlinear effective-mass model, aiming to include other important interactions (electron-electron and electron-phonon) not considered in previous sections. The interplay between disorder and nonlinearity is discussed in some extend. Finally, in Section 7 we will summarize and draw some conclusions.

2. MODEL OF DISORDERED SUPERLATTICES

2.1. Unintentional disorder

There exist several techniques, like scanning tunneling microscopy [10,19,20] and X-ray scattering [11], which have been applied in recent years to quantitatively determine structural properties of multilayers and SLs. Precise information about the nature and extend of defects at interfaces is now available. Following Mäder *et al.* [21], disorder in a SL can be classified into two categories, namely lateral and vertical. Lateral disorder occurs whenever one semiconductor protrudes into the other, forming chemically intermixed interfaces, steps and islands. As a consequence, the interface is not flat and translational symmetry in the plane perpendicular to the growth direction is broken. On the other side, vertical disorder is observed whenever layer thicknesses fluctuate around their nominal values. In such a case, translational symmetry along the growth direction is broken and electrons moving in this direction are reasonably well described by a Kronig-Penney model [22] with wells and barriers of random widths and heights. Compositional disorder due to different Al concentration in each $Ga_{1-x}Al_xAs$ layer can be also viewed as vertical disorder for ΔE_c takes random values over the whole SL. Unintentional disorder is likely to consists of both types of disorder [23,24].

Unintentional disorder appearing during growth in *actual* SLs depends critically on the growth conditions. Therefore, it seems to be extremely difficult to describe all possible experimental scenarios within the EFM. At first glance, one might use three-dimensional band-structure theories, but unfortunately large computational facilities are required to simulate the absence of periodicity. This shortcoming is even worse in the case of time dependent phenomena since equations are to be solved in space *and* time. Therefore, researchers usually assume some reasonable approximations in order to make models as simple as possible. In view of the theoretical simplicity of EFM, lateral imperfections are simulated by continuous potential profiles corresponding to averages in the planes perpendicular to the growth direction [25–30]. In what follows, we describe local excess or defect of monolayers by allowing the quantum well widths to fluctuate uniformly around their nominal values; this can be seen as substituting the nominal sharp width by an *average* along the parallel plane of the interface imperfections. Therefore, translational symmetry in the planes perpendicular to the growth direction is restored, this effective model being quasi-one-dimensional. Our approximation is valid whenever the mean free path of electrons is much smaller than the in-plane average size of protrusions as electrons only *see micro*-quantum-wells with small area and uniform thickness. Moreover, vertical disorder can also bd described in this way. Therefore, in the following, we will take the width of the nth quantum well to be $d_w^n = a(1 + W\epsilon_n)$, where W is a positive parameter measuring the maximum fluctuation, a is the nominal quantum well width, and ϵ_n's are uncorrelated random numbers distributed according to a uniform probability distribution

$$\mathcal{P}(\epsilon_n) = \begin{cases} 1, & \text{if } |\epsilon_n| < 1/2, \\ 0, & \text{otherwise.} \end{cases} \tag{1}$$

Therefore, each quantum well presents a slightly different value of its thickness and resonant coupling between electronic states of neighboring wells decreases. To keep the number of parameters to a minimum, we further assume that neither the barrier widths nor their heights fluctuate and then take $d_b^n = b$ and ΔE_c constant over the whole SL.

2.2. Envelope-function method

We focus now on electron states close to the bandgap. Since disorder is restricted along the growth direction in the above model, the eigenvalue $\mathbf{k}_\perp$ of the momentum perpendicular to this direction is constant of motion. Here x and y denote the coordinates in the plane perpendicular to the growth direction, z. The electron wave function is the product of a band-edge orbital (crystal Bloch function) with a slowly varying function. The latter can be factorized as $\exp(i\mathbf{k}_\perp \cdot \mathbf{r}_\perp)\psi(z)$, with $\mathbf{r}_\perp = (x, y)$. After inserting this ansatz into the Schrödinger equation, we arrive at the effective-mass equation for the envelope-function $\psi(z)$. For $\mathbf{k}_\perp = \mathbf{0}$ (nonzero values can be easily included in the calculations), the effective-mass equation for electrons takes the form

$$\left[-\frac{\hbar^2}{2}\frac{d}{dz}\frac{1}{m^*(z)}\frac{d}{dz} + V_{\mathrm{SL}}(z)\right]\psi(z) = E\psi(z). \tag{2}$$

The dependence of the effective-mass $m^*(z)$ upon the coordinate along the growth direction in GaAs-$Ga_{1-x}Al_xAs$ SLs is given as follows

$$m^*(z) = \begin{cases} m_b^*, & \text{if } |z - z_n| < b/2, \\ m_w^*, & \text{if } |z - z_n| > b/2, \end{cases} \quad (3)$$

for $z_{n-1} + b/2 < z < z_{n+1} - b/2$, where $m_b^* = (0.067 + 0.083x)m_0$, $m_w^* = 0.067m_0$, m_0 is the free-electron mass, and x is the Al fraction in the $Ga_{1-x}Al_xAs$ layer whose centre is located at z_n (here the index n runs over every barrier). Similarly, the SL potential can be written as

$$V_{SL}(z) = \sum_n V(z - z_n), \quad (4)$$

where we have defined

$$V(z - z_n) = \begin{cases} \Delta E_c, & \text{if } |z - z_n| < b/2, \\ 0, & \text{if } |z - z_n| > b/2, \end{cases} \quad (5)$$

Notice that the energy is measured from the bottom of the conduction-band in GaAs. Figure 2 presents the conduction-band edge profile $V_{SL}(z)$ in a disordered GaAs-$Ga_{1-x}Al_xAs$ SL. Let us comment that holes can be treated in a similar fashion.

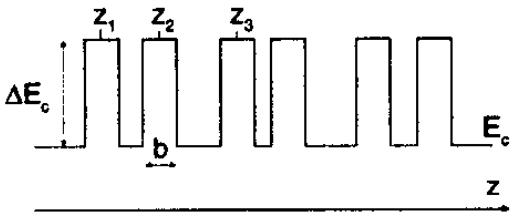

FIG. 2. Conduction-band edge profile in a disordered GaAs-$Ga_{1-x}Al_xAs$ SL. Barriers are assumed to have the same thickness b and height ΔE_c. The coordinate of the centre of the nth barrier is denoted by z_n.

3. ELECTRON TRANSMISSION ACROSS A DISORDERED SUPERLATTICE

3.1. Transfer matrix formalism

There exist at present simple, accurate and fast algorithms for numerically solving the EFM equations. In the absence of applied electric and magnetic fields, the SL potential is piecewise constant, corresponding to the various layers of different semiconductors. Since the local solution of the EFM equation is known, one can relate solutions at neighboring layers via appropriate boundary conditions [31]. Let us consider states below the barrier ($0 < E < \Delta E_c$), which are the most interesting ones to study quantum confinement effects. The corresponding envelope-function in the quantum well between the barriers centered at z_n and z_{n+1} is

$$\psi_n^w(z) = p_n^w e^{i\gamma(z - z_n - b/2)} + q_n^w e^{-i\gamma(z - z_n - b/2)}, \quad (6)$$

for $z_n + b/2 < z < z_{n+1} - b/2$. Here $\gamma^2 = 2m_w^* E/\hbar^2$, p_n^w and q_n^w are two constants to be determined later. Inside the nth barrier the envelope-function can be written

$$\psi_n^b(z) = p_n^b e^{-\eta z} + q_n^b e^{\eta z}, \quad (7)$$

for $z_n - b/2 < z < z_n + b/2$ and now we have defined $\eta^2 = 2m_b^*(\Delta E_c - E)/\hbar^2$. Here p_n^b and q_n^b are also constants.

Since $\psi(z)$ and $[m^*(z)]^{-1}d\psi(z)/dz$ are continuous at the interfaces (see e.g. [32]), we can elate the corresponding envelope-function

values at both sides of the nth barrier via the 2×2 transfer-matrix $M(n)$

$$\begin{pmatrix} p_n^w \\ q_n^w \end{pmatrix} = M(n) \begin{pmatrix} p_{n-1}^w \\ q_{n-1}^w \end{pmatrix} \tag{8a}$$

with

$$M(n) \equiv \begin{pmatrix} \alpha_n & \beta_n \\ \beta_n^* & \alpha_n^* \end{pmatrix}, \tag{8b}$$

whose elements are given by

$$\alpha_n = \left[\cosh(\eta b) + \frac{i}{2} \left(\frac{\gamma m_b^*}{\eta m_w^*} - \frac{\eta m_w^*}{\gamma m_b^*} \right) \times \sinh(\eta b) \right] \exp[i\gamma(z_n - z_{n-1} - b)], \tag{8c}$$

$$\beta_n = -\frac{i}{2} \left(\frac{\gamma m_b^*}{\eta m_w^*} + \frac{\eta m_w^*}{\gamma m_b^*} \right) \sinh(\eta b) \times \exp[-i\gamma(z_n - z_{n-1} - b)], \tag{8d}$$

α_n^* and β_n^* being the complex conjugate of α_n and β_n, respectively. Letting N be the total number of barriers, the transfer-matrix $T(N)$ of the SL is obtained as the product

$$T(N) = \prod_{n=N}^{1} M(n) \equiv \begin{pmatrix} A_N & B_N \\ B_N^* & A_N^* \end{pmatrix}. \tag{9}$$

The element A_N can be easily calculated recursively from the relationship [33]

$$A_n = \left(\alpha_n + \alpha_{n-1}^* \frac{\beta_n}{\beta_{n-1}} \right) A_{n-1} - \left(\frac{\beta_n}{\beta_{n-1}} \right) A_{n-2}, \tag{10}$$

supplemented by the initial conditions $A_0 = 1$, $A_1 = \alpha_1$. The knowledge of A_N enables us to obtain relevant quantities like the transmission coefficient at a given energy E, $\tau(E) = 1/|A_N|^2$. Notice that these expressions are valid for any arbitrary value of quantum wells thicknesses and, consequently, they can be used in perfect as well as in imperfect disordered SLs within the one-band framework in the absence of applied fields.

3.2. Time-dependent effective-mass method

We are also interested in the quantum diffusion of wave packets in unintentional disordered SLs. The equation which rules the evolution of the wave packet is the time-dependent effective-mass equation

$$i\hbar \frac{\partial \Psi(z,t)}{\partial t} = \mathcal{H}(z)\Psi(z,t), \tag{11}$$

where $\mathcal{H}(z)$ is the single-electron Hamiltonian given in (2). Different initial states are employed in order to explore the effect of the SL potential and energy components of the initial states [34]. Linear combinations of several Wannier functions are thought to represent initial wave functions that seem to arise in experiments [35–37]. In addition, traveling Gaussian initial wave functions are also studied, showing a reasonable description of the dynamical phenomena observed in experiments [38]. Thus, we will study the quantum dynamics of an initial Gaussian wave packet

$$\Psi(z,0) = \left(\frac{1}{2\pi\sigma^2} \right)^{\frac{1}{4}} \exp\left[\frac{ik_0 z - (z - z_0)^2}{4\sigma^2} \right], \tag{12}$$

impinging on the SL, where the mean kinetic energy is $\langle E \rangle = \hbar^2 k_0^2 / 2m^*$ and σ measures

the width of the initial electron wave packet. For simplicity we take a constant effective-mass, although more general situations can also be handled. The solution of Eq. (11) is given by

$$\Psi(z,t) = \exp\left(-\frac{i}{\hbar}\mathcal{H}(z)t\right)\Psi(z,0). \quad (13)$$

The finite difference representation of the exponential [39]

$$\exp\left(-\frac{i}{\hbar}\mathcal{H}(z)\delta t\right) = \frac{1-\frac{i}{2\hbar}\mathcal{H}(z)\delta t}{1+\frac{i}{2\hbar}\mathcal{H}(z)\delta t}, \quad (14)$$

where δt is the time step, provides a powerful and high-accurate numerical method [the roundoff error is $(\delta t)^3$]. In addition, it ensures probability conservation [34] which can be used at every time step as a first test of the accuracy of results. Boundary conditions read $\Psi(\infty,t) = \Psi(-\infty,t) = 0$ and we have chosen the SL sufficiently large to be sure that the wave packet never comes close to the boundaries.

3.3. Tunneling times and other dynamical tools

The subject of tunneling times is rich in contradictory definitions and results [40–42]. When we measure the *transmission time* t_T, we are trying to measure the time that a *transmitted* particle spends in the SL of length $\mathcal{L}$. The transmission time is straightforwardly obtained in the WKB limit for a ballistic electron,

$$t_T^{\mathrm{WKB}}(E) = \int_0^{\mathcal{L}} \sqrt{\frac{m^*}{2(\Delta E_c - E)}}\,\chi_w(z)\,dz + \int_0^{\mathcal{L}} \sqrt{\frac{m^*}{2E}}\,\chi_b(z)\,dz, \quad (15)$$

where $\chi_b(z)$ and $\chi_w(z)$ are the characteristic functions of the barriers and the wells, respectively. The mean dwell time t_{dw} is

$$t_{dw}(E) = \int_0^{\infty} dt \int_0^{\mathcal{L}} |\Psi(z,t)|^2\,dz, \quad (16)$$

and measures the average time spent by a wave packet in a given region of space. This time does not distinguish between particles transmitted or reflected, and hence the mean dwell time becomes the transmission time of a transmitted particle when most of the wave packet is transmitted, as was pointed out by Büttiker and Landauer [40] Numerically, it is simple to measure t_{dw}, and physically is a powerful tool to measure the density of states, since it can be shown that [42]

$$\rho(E) = \frac{1}{\pi\hbar}\,t_{dw}(E). \quad (17)$$

According to Ref. [42], this relationship is only valid for symmetrical one-dimensional structures. For non-symmetrical structures it should be replaced by $\rho(E) = \frac{1}{2\pi\hbar}\left[t_{dw}^r(E) + t_{dw}^l(E)\right]$, where the superscript refers to electrons coming from the right (superscript r) or from the left (superscript l). However, we have found no differences between $t_{dw}^r(E)$ and $t_{dw}^l(E)$ with the parameters used is most commons GaAs-$Ga_{1-x}Al_xAs$ SLs.

Nevertheless, as Eq. (15) is only valid in a perfect ballistic regime and the mean dwell time is only the transmission time in a idealized limit, we need to develop a method to measure t_T. This method is based on the

probability P_T that at time t the particle is found to have crossed the SL,

$$P_T(t) = \int_{\mathcal{L}}^{\infty} |\Psi(z,t)|^2 \, dz, \tag{18}$$

or the probability P_R that the particle is found to have been reflected back by the SL

$$P_R(t) = \int_{-\infty}^{0} |\Psi(z,t)|^2 \, dz. \tag{19}$$

To get an estimation of the spreading of the wave packet as a function of time we will use the time-dependent inverse participation ratio (IPR), defined as,

$$\mathrm{IPR}(t) = \int_{-\infty}^{\infty} |\Psi(z,t)|^4 \, dz. \tag{20}$$

In addition, we will study the centroid of the probability distribution

$$Z(t) = \int_{-\infty}^{\infty} z \, |\Psi(z,t)|^2 \, dz. \tag{21}$$

Usually the IPR is a good estimation of the spatial extent of electronic states. Delocalized states are expected to present small IPR (for long times IPR $\sim 1/\mathcal{L}$), while localized states have larger IPR.

4. SUPERLATTICES UNDER dc FIELDS

4.1. Electron transmission under dc electric fields

The transfer matrix method is based on the local solution of the effective-mass equation (2). The solution can be expressed in terms of plane waves in the absence of applied electric fields, as shown above in Section 3. However, as soon as some voltage is applied to the sample, the SL potential might include the potential due to the electric field $V_{\mathrm{SL}}(z) + \mathcal{V}(z)$. The electric potential field, $\mathcal{V}(z)$, is to be calculated self-consistently by solving the Poisson and effective-mass equations [43,44]. As a first approximation, it is usually assumed that the potential drop across the SL is linear, namely $\mathcal{V}(z) = -eFz$, where $-e$ is the electron charge and F is the electric field. Local solutions of the EFM equation are combinations of Airy functions and the transfer matrix method can be applied [45]. However, such an approach does not hold when the Poisson and effective-mass equations might be solved self-consistently since the electric potential is not linear. To overcome this shortcoming one must restore on numerical solutions. Below we show in detail a numerical method which is valid under broad general circumstances.

The transmission probability $\tau(E,V)$ at a given bias $V = F\mathcal{L}$ is obtained by discretizing the effective-mass equation (2) for the SL potential $V_{\mathrm{SL}}(z)$ plus the linear potential $-eVz/\mathcal{L}$ due to the applied electric field [46]. The electric field is assumed to be applied only on the SL whereas it vanishes at the contacts. We divide the interval $[0,\mathcal{L}]$ in a grid of points $\{z_k = ks\}$, where s is the integration step. The discretized form of the effective-mass equation (2) may be cast in the matrix form (assuming constant effective-mass for simplicity)

$$\begin{pmatrix} \psi(z_{k+1}) \\ \psi(z_k) \end{pmatrix} = P_k \begin{pmatrix} \psi(z_k) \\ \psi(z_{k-1}) \end{pmatrix}, \tag{22a}$$

where we have defined

$$P_k \equiv \begin{pmatrix} \mu_k & -1 \\ 1 & 0 \end{pmatrix}, \tag{22b}$$

and

$$\mu_k \equiv 2 + \frac{2m^* s^2}{\hbar^2}\left[V_{SL}(z_k) - \frac{eVz_k}{\mathcal{L}} - E\right], \tag{22c}$$

for brevity. This form is suitable for a transfer-matrix approach to solve the scattering problem. In fact, iterating this equation one obtains

$$\begin{pmatrix} \psi(z_{N_s+1}) \\ \psi(z_{N_s}) \end{pmatrix} = T(N_s) \begin{pmatrix} \psi(z_0) \\ \psi(z_{-1}) \end{pmatrix}. \tag{23}$$

$T(N_s) = P_{N_s} \cdots P_0$ is the global transfer matrix and N_s is the number of grid points in the SL. $T(N_s)$ is real and relates the wave function at both edges of the structure. The solution of the wave equation is the field-free region is given by

$$\psi(z_k) = \begin{cases} e^{iq_0 k} + re^{-iq_0 k} & k \le 0, \\ te^{iq_{\mathcal{L}} k} & k \ge N_s, \end{cases} \tag{24}$$

where

$$q_0 \equiv \sqrt{\frac{2m^* E s^2}{\hbar^2}}$$

and

$$q_{\mathcal{L}} \equiv \sqrt{\frac{2m^*(E+eV)s^2}{\hbar^2}}$$

for small s. Using (23) and (24), we find that the transmission coefficient is given by

$$\tau(E,V) = \frac{4\sin q_0 \sin q_{\mathcal{L}}}{D(E,V)}, \tag{25a}$$

with

$$\begin{aligned} D(E,V) \equiv\ & T_{11}^2 + T_{12}^2 + T_{21}^2 + T_{22}^2 \\ & + 2(T_{11}T_{12} + T_{21}T_{22})\cos q_0 \\ & - 2(T_{11}T_{21} + T_{12}T_{22})\cos q_{\mathcal{L}} \\ & - 2(T_{11}T_{22} + T_{12}T_{21})\cos q_0 \cos q_{\mathcal{L}} \\ & + 2\sin q_0 \sin q_{\mathcal{L}} \end{aligned} \tag{25b}$$

where the dependence of T_{ij} on N_s has been omitted for brevity. Taking into account that $T(k) = P_k T(k-1)$ and $T(0) = P_0$ we find the following recurrence relationships

$$\begin{aligned} T_{11}(k) &= \mu_k T_{11}(k-1) - T_{11}(k-2), \\ T_{12}(k) &= \mu_k T_{12}(k-1) - T_{12}(k-2), \\ T_{21}(k) &= T_{11}(k-1), \\ T_{22}(k) &= T_{12}(k-1), \quad k = 1, 2 \cdots N_s. \end{aligned} \tag{26}$$

In order to determine the transmission coefficient, these equations must be supplemented with the initial conditions $T_{ij}(-1) = \delta_{ij}$, $T_{11}(0) = \mu_0$, $T_{12}(0) = -1$, $T_{21}(0) = 1$ and $T_{22}(0) = 0$.

Once the transmission coefficient has been determined, some relevant magnitudes can be readily determined. For example, the j–V characteristic is a physical magnitude amenable of experimental verification. The current density at a given temperature T for a SL subject to a uniform electric field can be calculated within the stationary-state model [47] (see also Ref. [48] for further details)

$$j(V) = \frac{m^* e k_B T}{2\pi^2 \hbar^3} \int_0^\infty N(E,V)\tau(E,V)dE, \tag{27}$$

where V is the applied bias and k_B the Boltzmann constant. $N(E,V)$ accounts for the oc-

cupation of states in both sides of the device, according to the Fermi distribution function, and it is given by

$$N(E,V) = \ln\left(\frac{1+e^{(E_F-E)/k_BT}}{1+e^{(E_F-E-eV)/k_BT}}\right), \tag{28}$$

E_F being the Fermi level, which will be assumed to be located at the conduction-band edge of GaAs in what follows. The transmission probability $\tau(E,V)$ at a given bias V is obtained by means of Eq. (25).

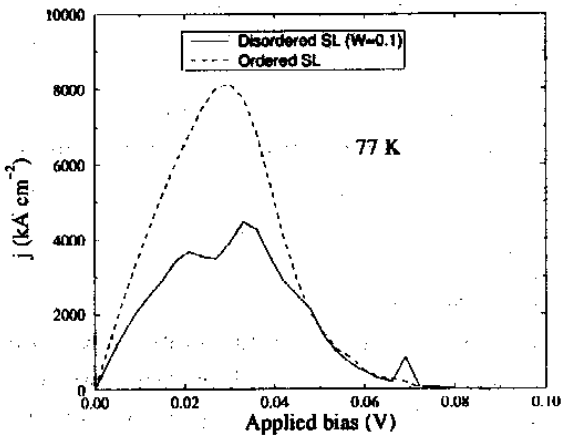

FIG. 3. j–V characteristic of ordered (dashed lines) and unintentionally disordered (solid lines) $GaAsAl_xGa_{1-x}As$ SLs at 77 K.

Figure 3 shows the j–V characteristic at 77 K for both ordered and unintentionally disordered ($W = 0.1$) SLs with 11 barriers of width 15 Å and 10 wells of width 90 Å. The effective–mass is assumed to be constant over the whole SL ($m^* = 0.067m_0$) and $\Delta E_c = 0.25$ eV. We observe the occurrence of negative differential resistance in both SLs, but the corresponding peak-to-valley ratios are quite different. In particular, the disordered SL displays peak-to-valley ratios two times smaller than the ordered one. It is important to mention that these results are based on the assumption of purely ballistic current regime across the SL. In a recent paper, Rauch *et al.* [49] have found that the coherence length in uniform GaAs-$Al_xGa_{1-x}As$ is about 150 nm, namely larger than the SL length we have studied (110 nm). Therefore, we can confidently admit coherent transport across the SL.

4.2. Semiclassical theory of Bloch oscillations

More than seventy years ago, Bloch started with the investigation of the motion of an electron wave packet with narrow distribution of moments in a periodic potential subject to an external applied electric field [50]. Work by Bloch was further clarified and elaborated by Zener [51]. It was suggested that the electron gains energy from the field, and moves in k and real spaces. This motion is determined by the acceleration theorem and the dispersion relation $E(k)$. For a nearest-neighbor tight-binding Hamiltonian in the one-band approximation, the dispersion relation is given by

$$E(k) = E_0 - \frac{\Delta}{2}\cos(kL), \tag{29}$$

where E_0 is the energy of the center of the band of width Δ. The momentum of the electron should change according to the following equation [50]

$$\hbar\frac{dk}{dt} = eF \tag{30}$$

Since the band structure is periodic in k, Zener pointed out that an electron which is not subject to scattering processes will perform an oscillatory motion in k space. This motion is accompanied by a periodic motion in real space, the so-called Bloch oscillations (BOs).

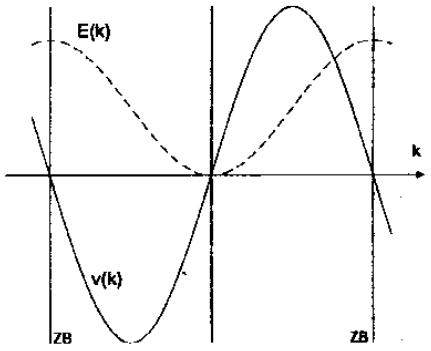

FIG. 4. Bloch oscillations in the semiclassical picture. An electron initially at $k = 0$ oscillates between the edges of the zone boundaries (ZB).

An illustration of BOs in k space in presented in Ref. [52] and it is shown in Fig. 4. The electron initially at $k = 0$ accelerates according to the acceleration theorem (30). The real space velocity (group velocity) $v(k) = \partial E(k)/\partial k$ vanishes at the edges of the Brillouin zone, the electron undergoes a Bragg reflection and reverts its real space velocity, thus performing an oscillatory motion of period (Bloch period)

$$\tau_B = \frac{h}{eFL}, \tag{31}$$

where L is the spacing of the underlying lattice, an real space amplitude [53]

$$A_B = \frac{\Delta}{2eF}, \tag{32}$$

the coherent carrier motion being restricted to a region of length $2A_B$. The values of the period and the amplitude are rather independent of the particular details of the band structure.

The above semiclassical description of wave packet motion evolution cannot be naively applied in SLs for the wave packet created in experiments do not meet the semiclassical smoothness of its Fourier transform. Excitonic effects could also be important and the one-particle description might be incorrect [53]. The semiclassical results are improved by directly solving the effective-mass equation for the SL subject to a uniform electric field [53,54]. However, SLs are far from being ideal, as we mentioned in the Introduction; different scattering mechanisms (surface roughness, impurities) and many-body effects (electron-electron and electron-phonon interactions) might be included in the models, which turn out to be rather complex to allow for analytical solutions. Thus, numerical results may help to understand experimental results.

4.3. Observation of Bloch oscillations

The relaxation time τ_R of carriers should be larger than τ_B if BOs are to be detected in an experiment. Therefore, from Eq. (31) it becomes clear that the applied electric field F might then satisfy the condition

$$F > \frac{h}{e\tau_R L}. \tag{33}$$

This condition requires extremely nigh values of the electric field in bulk materials. Fortunately, SLs have both much larger lattice

period L and relaxation times τ_R than bulk materials.

Several years ago, von Plessen and Thomas proposed a method for observing BOs in the time domain [55]. These author suggested an experimental method that consists of measuring the spontaneous photon-echo signal in a time-resolved four-wave mixing experiment. The first experiment observing BOs by optical excitation was reported by Feldmann *et al.* [35]. Later experiments showed clear oscillations in the four-wave mixing signal [36]. A rather detailed study of BOs and their dependence on the applied field, miniband width, lattice temperature, and excitation conditions was carried out by Leisching *et al.* [52]. Moreover, it has been possible to show that the amplitude of photogenerated wave packets can be controlled between true Bloch oscillations —with center-of-mass motion— and symmetric breathing modes —with no center-of-mass motion but width fluctuation— in semiconductor SLs [56]. Another remarkable example of recent advances has been given by Lyssenko *et al.* [57]: The oscillating Bloch wave packet creates a small dipole field which can be detected by means of the field shift of the Wannier-Stark ladder transitions. The absolute spatial displacement of Bloch-oscillating electrons is then measured. These authors found that the electron wave packet performs a sinusoidal oscillation whose amplitude is very close to the theoretical prediction including excitonic effects [53]. See Ref. [58] for a recent review on interband optical investigation and related experimental topics of BOs in SLs.

4.4. Dephasing induced by weak disorder

Inelastic scattering by phonons, deviations from SLs perfect periodicity due to unintentional imperfections, intraband scattering, interminiband transitions, and scattering by impurities severely reduce the quantum coherence required for the observation of BOs. The periodic motion of wave packet under BOs conditions persists until Bloch electron loses energy gained from the field through scattering processes. However, even in the most favorable experimental conditions, τ_R is not much larger than τ_B and thus only a few BOs are usually observed.

The origin of such loss of quantum coherence in actual devices is far from being understood and, at present, there is much debate about the role played by different scattering mechanisms in those processes. In this regard, Plessen *et al.* [59] found that quantum coherence is lost after a few BOs in 30 Å GaAs/30 Å $Ga_{0.7}Al_{0.3}As$ SLs, a fact which was attributed to scattering by LO phonons. On the other hand, theoretical studies point out that under most experimental conditions interminiband transitions are negligible and, consequently, cannot be responsible for the signal decay [60]. Furthermore, Plessen *et al.* [59] conclude from their experimental results that the threshold electric field is higher for SLs with Δ larger than the energy of LO phonons, $E_{LO} = 36\,\text{meV}$. They explain this dependence by assuming that LO phonon emission is excluded when $\Delta < E_{LO}$. On the contrary, Leisching *et al.* [52] detected up to six BOs but they did not observe any sign of a phonon threshold in SLs with Δ ranging from 13 up to 46 meV. These authors argued that the reduced sample quality of Ref. [59] could be the responsible for the threshold.

From the above discussions, it becomes clear that understanding the interplay be-

tween the electric field and the imperfections of the SLs is crucial to elucidate the discrepancies among different groups, either to pinpoint its relevance or to exclude it [38,61]. Here we present a complete study of the effects of interface roughness on the BOs. We study the dynamical behavior of intentionally disordered SLs subject to a dc electric field by measuring the time-dependent IPR (20) and the position of the centroid of the wave packet (21). These quantities will allow us to conclude that the assumption of weak disorder is enough to explain all the available experimental data, thus firmly connecting the dephasing of BOs to the quality of the sample.

We have considered the same SLs as those ones used in previous experiments [52,59]. In particular, we present here results for the first one of these SLs, i.e., 100 periods of 30 Å GaAs and 30 Å $Ga_{0.7}Al_{0.3}As$ [59]. In this case, the conduction-band offset is $\Delta E_c = 0.25\,\text{eV}$. Samples are labeled according to their nominal period length $L = a + b$, namely 60Å SL. Similar results are obtained with the other SLs like the 84, 97, or 128 Å ($b = 17$ Å, $a = 67$, 80 and 111 Å, respectively), i.e., the ones reported by Leisching *et al.* [52], although we do not present here these results for brevity. We have straightforwardly calculated the miniband-width for the 60Å SL obtaining $\Delta = 90\,\text{meV}$, being larger than E_{LO}.

We study applied electric fields in the range from 5 up to 20 kV/cm. The fluctuation parameter runs from $W = 0$ (ordered SL) up to $W = 0.20$ (strongly disordered SL). Figure 5 displays the centroid position of the wave packet in the 60 Å SL for $F = 10\,\text{kV/cm}$ and different values of the unintentional disorder. The initial Gaussian wave packet is located in the centermost quantum well with $\sigma = 300$ Å. In Fig. 5(a), for an ordered SL, we observe the occurrence of very well defined BOs with amplitude $2A = 900$ Å and period $\tau_B = 0.7\,\text{ps}$, in excellent agreement with the semiclassical predictions $2A_B = 900$ Å and $\tau_B = 0.69\,\text{ps}$.

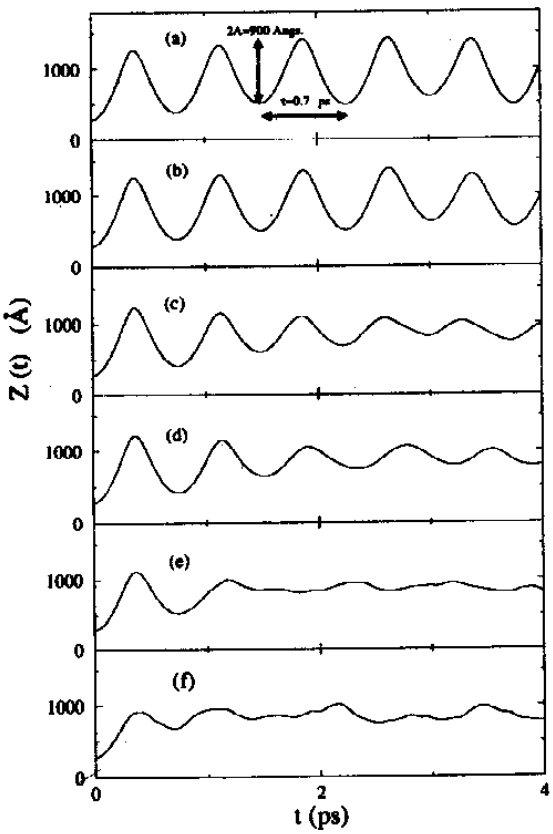

FIG. 5. Centroid of an initial Gaussian wave packet with $k_0 = 0$ and $\sigma = 300$ Å as a function of time in 60 Å SLs. The applied electric field is $F = 10\,\text{kV/cm}$. From top to bottom (a) $W = 0$, (b) 0.01, (c) 0.03, (d) 0.05, (e) 0.10, and (f) 0.20.

Notice, however, that the perfect oscillatory pattern detected in ordered SLs (upper panel) is progressively destroyed upon increasing the degree of disorder as seen in

the rest of panels in Fig. 5, for $W = 0.01$, 0.03, 0.05, 0.10, and 0.20. It is most important to mention here that the results do not depend on the particular realization of disorder. We note that those values correspond, if we assume that a monolayer width of this type of SLs is about 3Å, to a maximum excess of defect of less than one monolayer ($W = 0.01$ and 0.03), one monolayer ($W = 0.05$), two monolayers ($W = 0.10$) and four monolayers ($W = 0.20$). The disorder induces a decrease of the amplitude of the oscillations and, besides, it produces a progressive dephasing comparing with the ordered case. In the strong disorder case no signs of BOs are found. This fact can be explained by the absence of translational invariance at flatband and, consequently, by scattering of electrons with the random potential. Similar results are obtained with the SLs reported by Leisching *et al.* [52].

We can achieve better resolution of the BOs period and the influence of the disorder by means of the IPR. The upper panel of Fig. 6 presents the results for the IPR of the ordered 60 Å SL when the initial Gaussian wave packet is located in the centermost quantum-well with $\sigma = 20$ Å. The electric field is $F = 10\,\mathrm{kV/cm}$. In the absence of imperfections, the IPR displays a periodic pattern with marked peaks at times $t_n = n\tau_B$, where n is any arbitrary, nonnegative integer and $\tau_B = 0.7\,\mathrm{ps}$. This means that the initial localized state is recovered after this time. Results corresponding to disordered SLs with the same initial conditions as before are shown in the remaining panels of Fig. 6, confirming that BOs progressively disappear on increasing the degree of disorder.

From the above results we are led to the

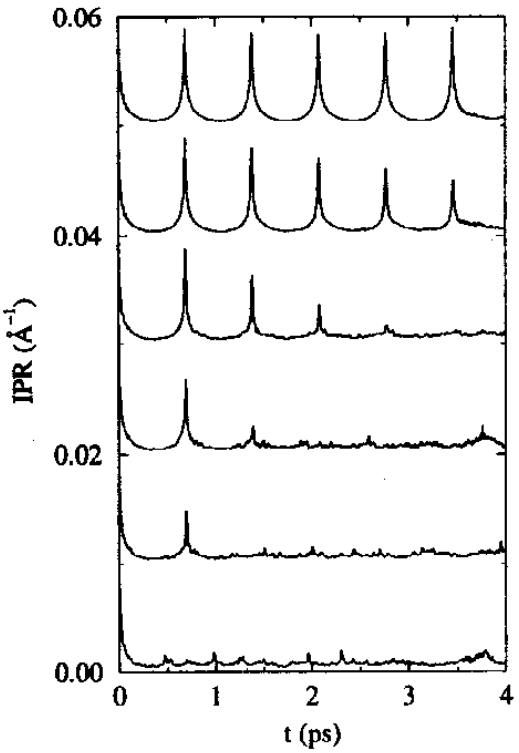

FIG. 6. IPR as a function of time for an initial Gaussian wave packet with $\sigma = 20$ Å, subject to an electric field $F = 10\,\mathrm{kV/cm}$ in 60 Å SLs. From top to bottom $W = 0$, 0.01, 0.03, 0.05, 0.10, and 0.20. For clarity, curves are progessively shifted 0.01 Å upwards.

conclusion that there exists a characteristic scattering time τ_{dis} after which BOs are destroyed even by weak disorder. Moreover, it is readily observed in Fig. 6 that τ_{dis} decreases upon increasing the degree of disorder. However, the above results have been obtained for a fixed value of the electric field, but clearly a meaningful definition of the scattering time should be independent of the value of the electric field. To check the validity of the introduced τ_{dis} we have studied the IPR for different values of the applied electric field at a given degree of disorder. Rep-

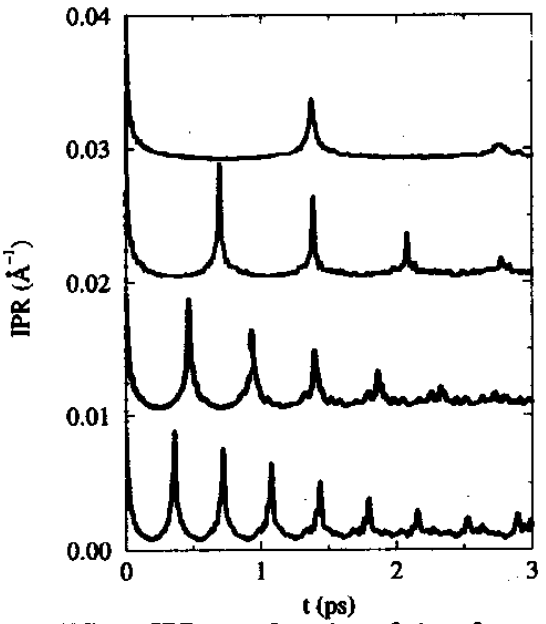

FIG. 7. IPR as a function of time for an initial Gaussian wave packet with the same parameters as in Fig. 6, placed in a 60 Å SLs with $W = 0.03$. From top to bottom $F = 5$, 10, 15, and 20 kV/cm. For clarity, curves are progessively shifted 0.01 Å upwards.

resentative results are presented in Fig. 7 for $W = 0.03$ (on average less than one monolayer) and $F = 5$, 10, 15 and 20 kV/cm.

From this plot we can roughly estimate that $\tau_{\rm dis} \simeq 2.5$ ps for all values of the electric field. Thus, this scattering time plays the same role as the scattering time arising from inelastic interactions, in the sense that $\tau_{\rm B}$ must be kept smaller than $\tau_{\rm dis}$ to observe BOs. Interestingly, this value is the same as that obtained in the experiments of Plessen *et al.* [59]. The scattering time increases when the minibandwidth decreases, for the same amount of disorder, and values obtained with our model turn out to be perfectly consistent with all the experimental data [35,52,62].

5. SUPERLATTICES UNDER TIME DEPENDENT ELECTRIC FIELDS

5.1. Theory of Rabi oscillations

The oscillations of a two level system between the ground and excited states in the presence of a strong resonant driving field, called Rabi oscillation (RO), are discussed in textbooks [63] as a topic of time-dependent perturbation theory. It was first treated by Rabi [64] in the context of molecular beam magnetic resonance experiments [65]. This author considered a two state system with ground state energy E_0 and excited state E_1 in the presence of a harmonic perturbation. If the frequency of the perturbation matches roughly the spacing between the two levels, the system undergoes oscillations with a frequency Ω_R which is much smaller than the excitation frequency $\omega_{\rm ac}$. The so called Rabi frequency depends on the mismatch $\delta\omega \equiv (E_1 - E_0)/\hbar - \omega_{\rm ac}$ between the level spacing and the excitation frequency, and on the matrix element F_{10} of the perturbation $\Omega_R = \left(\delta\omega^2 + |F_{10}|^2/4\hbar^2\right)^{1/2}$. If the system is initially in the ground state, transitions between the ground and the excited state will occur with a period $T_R = 2\pi/\Omega_R$ as time evolves.

Rabi oscillations were observed in magnetic resonance experiments in bulk materials [66]. More recently, related phenomena were detected in semiconductor heterostructures. By examining the interaction of two copropagating ultrafast optical pulses in a semiconductor multiple quantum well, Cundiff *et al.* [67] have experimentally determined the temporal dependence of the induced polarization and concluded that the

optically induced density went through a maximum. These authors claimed that such phenomena are a manifestation of Rabi flopping [68] in semiconductors. Martin and Berman have proposed a switching nanodevice based on Rabi oscillation [69]. Resonant photon-assisted tunneling through a double quantum dot has been theoretically studied using the Keldysh nonequilibrium Green function technique by Stafford and Wingreen [70]. When driven on resonance, the system was shown to function as an efficient electron pump due to Rabi oscillation between the dots.

Therefore, the following question arises: is this naive description valid for a real SL? SLs present Bloch minibands with several states each one. Thus, it is not clear whether transitions between two minbands can be correctly described as a a pure two state system.

5.2. Rabi oscillations in superlattices

Recently, Zhao *et al.* have analytically investigated a tight-binding model of a two-band system in time-dependent ac-dc field in the weak coupling limit [71]. They identified ROs between Bloch bands under resonant conditions, which reveal the existence of quasi-energy bands and fractional Wannier-Stark ladders. However, the tight-binding approximation presents some limitations to describe actual SLs when the coupling between neighbor sites is not weak. Thus, in order to experimentally access the validity of theoretical predictions, we shall use a more realistic model based on the time-dependent effective-mass method [72]. We start with

$$i\hbar\frac{\partial\Psi(z,t)}{\partial t} = \left[-\frac{\hbar^2}{2m^*}\frac{d^2}{dz^2} + V_{\rm SL}(z) - eFz\sin(\omega_{\rm ac}t)\right]\Psi(z,t), \quad (34)$$

where F and $\omega_{\rm ac}$ are the strength and the frequency of the ac field.

The band structure at $F = 0$ is computed using the finite-element method [73]. The eigenstate j of the miniband i ($i = 0, 1, \ldots$) with eigenenergy $E_i^{(j)}$ is denoted as $\psi_i^{(j)}(z)$. A good choice for the initial wave packet is given by a linear combination of the eigenstates belonging to the first miniband. For the sake of clarity we have selected as the initial wave packet $\Psi(z,0) = \psi_i^{(j)}(z)$, although we have checked that this assumption can be dropped without changing our conclusions. The subsequent time evolution of the wave packet $\Psi(z,t)$ is calculated numerically by means of the implicit integration scheme given in Section 3.2 (see also Ref. [73]). In addition to $\Psi(z,t)$ we also compute the probability of finding an electron, initially in the state $\Psi(z,0) = \psi_i^{(j)}(z)$, in the state $\psi_k^{(j)}(z)$. This probability is given by

$$P_{ik}^{(j)}(t) = \int_{-\infty}^{\infty} dz\, \Psi^*(z,t)\psi_k^{(j)}(z). \quad (35)$$

We present here results for a SL with 10 periods of 100 Å GaAs and 50 Å $Ga_{0.7}Al_{0.3}As$ with $\Delta E_c = 0.25\,\text{eV}$. We consider electric fields from 12.5 up to 100 kV/cm as typical values. Figure 8(a) displays $P_{01}^{(5)}(t)$ with $F = 25\,\text{kV/cm}$ at the resonant frequency $\omega_{\rm ac} = (E_1^{(5)} - E_0^{(5)})/\hbar = 24\,\text{THz}$. In this way, we are monitoring the transitions between the central state ($j = 5$) in the first miniband to the central state in the second

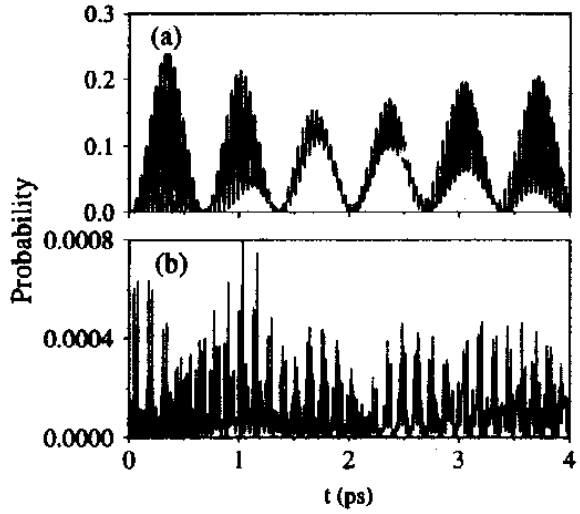

FIG. 8. Probability of finding an electron, initially situated in $\psi_0^{(5)}(z)$, in the state $\psi_1^{(5)}(z)$ as a function of time for $F = 25\,\mathrm{kV/cm}$, when the ac field (a) is tuned to the resonant frequency $\omega_{ac} = 24\,\mathrm{THz}$ and (b) is out of resonance $\omega_{ac} = 16\,\mathrm{THz}$. Notice the different vertical scales.

miniband as a function of time. We observe the occurrence of very well defined ROs when the ac field is tuned to the resonant frequency with an amplitude close to 0.25. Summing up the probabilities of the rest of states in the second miniband, the probability of finding the electron in this band is very close to unity ($\sim$ 0.99). The frequency of the ROs, obtained performing the fast Fourier transform (FFT) of $P_{01}^{(5)}(t)$ is $\omega_R = 3\,\mathrm{THz}$. The probability $P_{01}^{(5)}(t)$ is dramatically reduced when the ac driving field is out of resonance, as shown in Figure 8(b) for $\omega_{ac} = 16\,\mathrm{THz}$. The FFT of these data reveals no specific features besides the peak at the driving frequency ω_{ac}.

In a pure two-level system, a straightforward calculation yields $\omega_R = |F_{01}|/\hbar$. Thus, ω_R is linear in the electric field in a pure two-level system. Although the SL is not a pure two-level system, we realize that this linear dependence still holds, as we can see in Fig. 9.

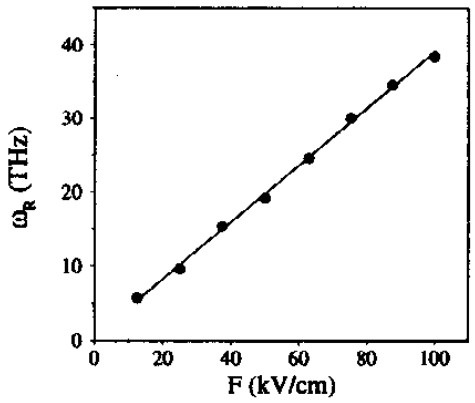

FIG. 9. Rabi frequency as a function of the electric field when the driving frequency is tuned to the resonant frequency $\omega_{ac} = 24\,\mathrm{THz}$.

5.3. Effects of interface roughness

The presence of imperfections introduced during growth processes should also be taken into account. Since ROs are a coherent phenomenon, unintentional disorder will affect them. From the viewpoint of applications, it is most important to elucidate whether ROs are to be detected in actual devices. To answer this question we consider again the model of disordered SL proposed in Section 2.

Figure 10 displays $P_{01}^{(5)}(t)$ with $F = 50\,\mathrm{kV/cm}$ at the resonant frequency $\omega_{ac} = 24\,\mathrm{THz}$ for both ordered ($W = 0$) and unintentionally disordered ($W = 0.03$, namely less than one monolayer) SLs. Notice that the perfect oscillatory pattern detected in perfect SLs is completely altered when we introduce a small amount of disorder. The disorder induces both a decrease of the amplitude of the oscillations and a progressive dephasing comparing with the ideal ordered case. This fact can be explained by scatter-

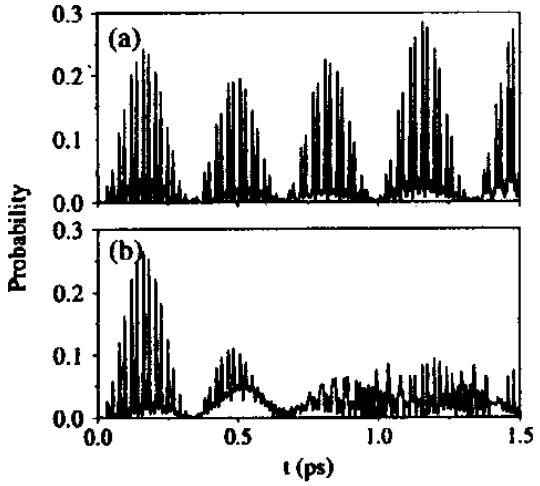

FIG. 10. Probability of finding an electron, initially situated in $\psi_0^{(5)}(z)$, in the state $\psi_1^{(5)}(z)$ as a function of time for $F = 50\,\mathrm{kV/cm}$, when the ac field is tuned to the resonant frequency $\omega_{ac} = 24\,\mathrm{THz}$ with (a) $W = 0$ (ordered SL) and (b) $W = 0.03$ (unintentionally disordered SL).

ing of electrons with the random potential.

From the above results we conjecture that there exists a characteristic scattering time τ_{dis} related to the amount of disorder in the sample, after which ROs are destroyed by disorder. Moreover, it is readily observed that τ_{dis} decreases upon increasing the degree of disorder. However, the above results have been obtained for a fixed value of the electric field. To check the validity of the proposed τ_{dis} we have studied $P_{01}^{(5)}(t)$ for different values of the ac field strength with the same amount of disorder. Typical results are presented in Fig. 11 for $W = 0.03$ and $F = 25$, 50 and $100\,\mathrm{kV/cm}$. From this plot we can roughly estimate that $\tau_{dis} \simeq 0.75\,\mathrm{ps}$ for all values of the electric field. Thus, this scattering time plays the same role as the scattering time arising from inelastic interactions, in the sense that the period of ROs must be kept smaller than τ_{dis} to be observed. The behavior of ROs is very similar to the case when disorder is absent for $t < \tau_{dis}$. Moreover, performing the FFT of $P_{01}^{(5)}(t)$ for different values of the electric field, we obtain that ω_R shows a linear dependence with the field, as it is expected from perturbation theory. The difference between the values of ω_R of perfect and imperfect SLs for $t < \tau_{dis}$ is negligible.

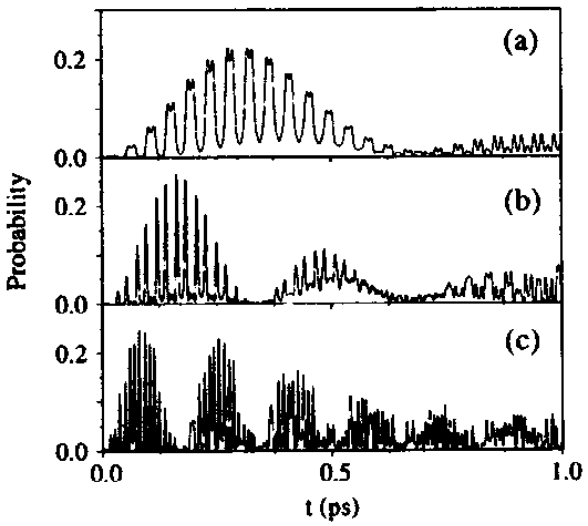

FIG. 11. Probability of finding the electron in the state $\psi_1^{(5)}(z)$ as a function of time for $W = 0.03$, $\omega_{ac} = 24\,\mathrm{THz}$ and (a) $F = 25$, (b) 50 and (c) $100\,\mathrm{kV/cm}$.

Figure 12 shows the integrated probability density in the right part of the SL, defined in (18), for (a) $W = 0$ and (b) 0.03. Solid lines are the results in the resonant regime $\omega_{ac} = 24\,\mathrm{THz}$, whereas dashed lines are the results for $\omega_{ac} = 32\,\mathrm{THz}$ (out of resonance). We can see that the tunneling probability is negligible when the ac field frequency is not very close to the resonant one. When ω_{ac} is close to the resonant frequency, the wave function is therefore emitted by *bursts* from

the SL region every time a RO has been completed. We can see that this phenomenon is also observed for the imperfect SL for times smaller than τ_{dis}.

Finally, some words about the experimental conditions to observe the theoretical findings are in order. Nowadays a high-power terahertz ac field can be generated in a free-electron laser [74]. A straightforward way to observe ROs in SL experimentally is to detect the radiation at the frequency ω_R emitted by the oscillating dipole associated with the RO when the SL is driven by the ac field at the resonant frequency.

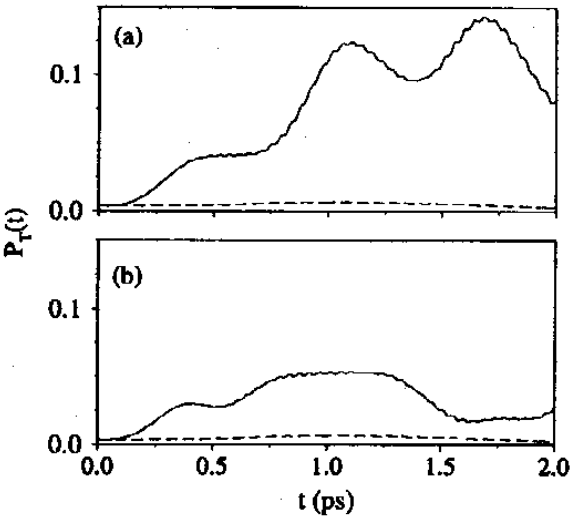

FIG. 12. $P_T(t)$ as function of time when $F = 50\,\mathrm{kV/cm}$, for (a) $W = 0$ and (b) 0.03. Solid lines are the results in the resonant regime $\omega_{ac} = 24\,\mathrm{THz}$, whereas dashed lines are results for $\omega_{ac} = 32\,\mathrm{THz}$ (out of resonance).

6. INTERPLAY BETWEEN DISORDER AND NONLINEAR EFFECTS

6.1. Electron transmission across superlattices: Nonlinear-effects

In semiconductor nanostructures there are several scattering mechanism that could result in a reduction of the carrier coherence. An example of inelastic scattering events is electron-electron interaction, in which the energy of the tunneling electron changes and the phase memory is lost. The influence of such many-body effects on SL has recently attracted considerable attention. Presilla *et al.* [75] pointed out the possibility of nonlocal effective nonlinearities due to many-body interactions in electron transport through semiconductor heterostructures. Several results have been obtained using this mean field analysis such as quantum chaos [76] and nonlinear oscillations [77–79]. Loosely speaking, this kind of treatment could be regarded as similar to Hartree-Fock and other self-consistent techniques, which substitute many-body interactions by a nonlinear effective potential. It has to be stressed, however, that the nonlocal interaction might not be the most suitable one in many contexts (e.g., when wells are wide) because it does not take into account the spatial variation of the effective potential.

To consider the electron-electron interaction we write a generalized effective-mass equation modifying Eq. (2) that now has the form

$$\left[-\frac{\hbar^2}{2}\frac{d}{dz}\frac{1}{m^*(z)}\frac{d}{dz}+V_{SL}(z)-eFz\right.$$

$$+\tilde{\alpha}|\psi(z)|^2\Big]\psi(z) = E\psi(z). \qquad (36)$$

with $\tilde{\alpha} = \alpha\,\Delta E_c\,L$ where ΔE_c is the conduction band offset, L is the SL period and α is the dimensionless nonlinear coupling constant.

To obtain the transmission coefficient we develop a similar approach to that given in Ref. [80]. For simplicity we take a constant effective-mass over the whole SL. As usual in scattering problems, we assume an electron incident from the left and define the reflection, r, and transmission, t, amplitudes by the relationships

$$\psi(z) = \begin{cases} e^{ik_0 z} + re^{-ik_0 z}, & z < 0, \\ te^{ik_{\mathcal{L}} z}, & z > \mathcal{L}, \end{cases} \qquad (37)$$

where we have introduced the notation $k_0^2 = 2m^*E/\hbar^2$ and $k_{\mathcal{L}}^2 = 2m^*(E + eF\mathcal{L})/\hbar^2$. The transmission coefficient is computed as $\tau = (k_{\mathcal{L}}/k_0)|t|^2$. Now we define $\psi(z) = (|t|\sqrt{k_{\mathcal{L}}})Q(z)\exp[i\zeta(z)]$, where $Q(z)$ and $\zeta(z)$ are real functions. Inserting this factorization in Eq. (36) we have [81]

$$\frac{d\zeta(z)}{dz} = Q^{-2}(z) \qquad (38)$$

and

$$-\frac{\hbar^2}{2m^*}\left(\frac{d^2Q(z)}{dz^2} - \frac{1}{Q^3(z)}\right) + \Big[V_{\mathrm{SL}}(z) - eFz - E\Big]\,Q(z) = 0. \qquad (39)$$

This nonlinear differential equation must be supplemented by appropriate boundary conditions. However, using Eq. (37) this problem can be converted into a initial conditions equation. In fact, it is straightforward to prove that

$$Q(\mathcal{L}) = k_{\mathcal{L}}^{-1/2}, \quad \left.\frac{dQ(z)}{dz}\right|_{z=\mathcal{L}} = 0, \qquad (40)$$

and that the transmission coefficient is given by

$$\tau = \frac{4k_0Q^2(0)}{1 + 2k_0Q^2(0) + k_0^2Q^4(0) + Q^2(0)Q_z^2(0)}, \qquad (41)$$

where $Q_z(0) = dQ(z)/dz|_{z=0}$. Hence, we can integrate numerically (39) with initial conditions (40) backwards, from $z = \mathcal{L}$ up to $z = 0$, to obtain $q(0)$ and $q_z(0)$, thus computing the transmission coefficient for given incoming energy E and applied voltage $V = F\mathcal{L}$. Once the transmission coefficient has been computed, and recalling that contacts are linear media, the tunneling current density at a given temperature T for the SL can be calculated within the stationary-state model with Eq. (27). As an example we have considered a symmetric GaAs-$Ga_{0.65}Al_{0.35}As$ double-barrier structure with $\mathcal{L} = 3d_w = 150\,\text{Å}$, and thus $L \equiv 2d_w$ in this case. The conduction-band offset is $\Delta E_c = 0.25\,\text{eV}$. In the absence of applied electric field and nonlinearities, there exists a single, very narrow resonance with $\tau \sim 1$ below the top of the barrier, with an energy of $\sim 81\,\text{meV}$, and hence the well supports a single quasi-bound state. Figure 13 shows the transmission coefficient as a function of the incoming energy for different values of the nonlinear coupling α (a) 0 and 10^{-4}, (b) 10^{-3} and (c) 10^{-2}, at zero bias. Insets show the effective potential the conduction-band profile.

It is clear that the resonances are shifted to energies higher than in the noninteracting case. The shift is produced by the accumula-

tion of charge in the well. These results are in very good agreement with self-consistent calculations [82,83] and reproduces the observed charge accumulation in the barriers, close to the heterojunctions, and in the center of the wells, obtained in the Hartree approximation [7]. Then we have shown that the effective nonlinear interaction we have introduced captures the essential physics of electron-electron interaction in resonant tunneling processes in a very simple way.

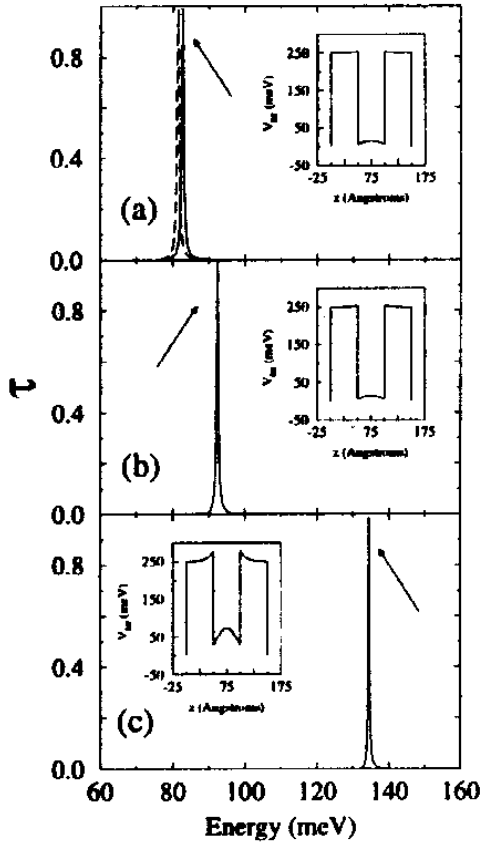

FIG. 13. Transmission coefficient τ as a function of the electron energy at zero bias for (a) $\alpha = 10^{-4}$, (b) 10^{-3}, and (c) 10^{-2}. For comparison, dashed line indicates in (a) the result for $\alpha = 0$. Insets show the conduction-band profile.

6.2. Nonlinear dynamics in superlattices under ac-fields

In the Sections 4.4 and 5.3 we investigate the dephasing effects of unintentional disorder in coherent phenomena as BOs and ROs. Now we want to study other decoherence processes producing the observed fast dephasing of coherence phenomena in SL, and more specifically in the interplay between the growth imperfections (disorder) and many-body effects as the electron-electron interaction. The interplay between the effects of disorder and many-body effects on electronic properties is a long-standing problem in solid-state physics. Probably one of the most promising ways to gain insight into this intricate problem is to combine the actual state-of-the-art of the molecular beam epitaxy, which allow us to grow samples with monolayer perfection and consequently with well-characterized disorder, with coherent oscillations that are extremely sensitive to imperfections and nonlinear effects.

Our model is based in the time-dependent effective-mass method. The envelope function for the electron wave packet satisfies the following quantum evolution equation

$$i\hbar\frac{\partial\Psi(z,t)}{\partial t} = \left[-\frac{\hbar^2}{2m^*}\frac{d^2}{dz^2} + V_{\rm NL}(z,t)\right]\Psi(z,t), \qquad (42)$$

We consider two approaches to the nonlinear potential $V_{\rm NL}(z,t)$ in Eq. (42). On the one hand we take into account the model described above, where $V_{\rm NL}(z,t)$ is

$$V_{\rm NL}(z,t) = V_{\rm SL}(z) - eF_{\rm ac}z\sin(\omega_{\rm ac}t)$$

$$+ \tilde{\alpha}_{\rm loc}|\Psi(z,t)|^2, \qquad (43)$$

$F_{\rm ac}$ and $\omega_{\rm ac}$ being the strength and the frequency of the ac field respectively. We define $\tilde{\alpha}_{\rm loc} = \alpha_{\rm loc}\,\Delta E_c\,L$ where ΔE_c is the conduction-band offset, L is the SL period and all the nonlinear physics is contained in the dimensionless coefficient $\alpha_{\rm loc}$ which we discuss below. There are several factors that configure the nonlinear response to the tunneling electron. We want to consider only the repulsive electron-electron Coulomb interactions, which should enter the effective potential with a positive nonlinearity, i.e., the energy is increased by local charge accumulations, leading to a positive sign for $\alpha_{\rm loc}$.

On the other hand, we have considered a different approach by solving self-consistently the Schrödinger and Poisson equations obtaining a Hartree-like potential [84]. In this context, the nonlinear potential is,

$$V_{\rm NL}(z,t) = V_{\rm SL}(z) - eF_{\rm ac}z\sin(\omega_{\rm ac}t) + \tilde{\alpha}_{\rm self}V_H(z,t), \qquad (44)$$

where now V_H it is obtained by solving the Poisson equation for the density of charge $|\Psi(z,t)|^2$, and we define the coupling coefficient as $\tilde{\alpha}_{\rm self} = \alpha_{\rm self}\,\Delta E_c\,L$, where $\alpha_{\rm self}$ is the dimensionless nonlinear coupling constant.

We present here results for a SL with 10 periods of 100 Å GaAs and 50 Å $Ga_{0.7}Al_{0.3}As$ with conduction-band offset 0.30 eV and $m^* = 0.067m_0$. The time and spatial mesh used in the simulations are 4×10^{-16} seconds and 1 Å; we have checked that our numerical results are not affected by these particular values. To illustrate the effects of the nonlinear coupling we show in Fig. 14 the conduction-band profile for a perfect SL

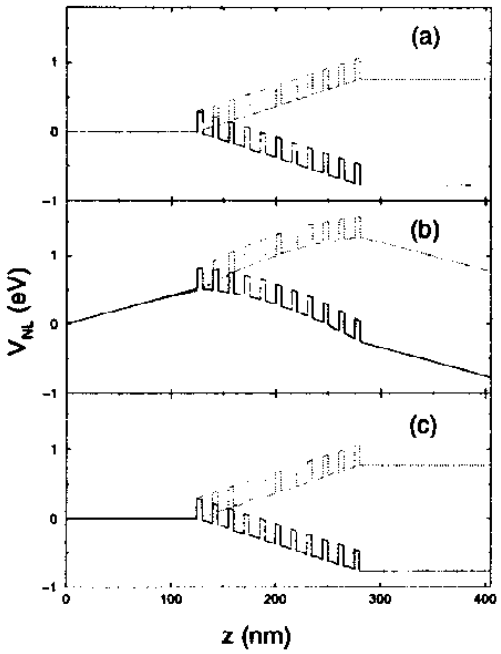

FIG. 14. Conduction-band profile for a perfect SL ($W = 0$) at $t = 0.4$ (solid lines) and 1.2 ps (dashed lines) for (a) the linear case and modeling the electron–electron interaction with (b) the self-consistent method ($\alpha_{\rm self} = 10^{-3}$) and with (c) the local model ($\alpha_{\rm loc} = 10$).

($W = 0$) at $t = 0.4$ (solid lines) and 1.2 ps (dashed lines) when the ac field is tuned to the resonant frequency $\omega_{\rm ac} = (E_1^{(5)} - E_0^{(5)})/\hbar = 24$ THz, for (a) the linear case and modeling the electron–electron interaction with (b) the self-consistent method ($\alpha_{\rm self} = 2.2 \times 10^{-5}$) and with (c) the local model ($\alpha_{\rm loc} = 0.22$).

In Fig. 15 we plot the probability of finding an electron, initially situated in $\psi_0^{(5)}(z)$, in the state $\psi_1^{(5)}(z)$ of a perfect SL ($W = 0$) as a function of time when the ac field is tuned to the resonant frequency, for different values of the nonlinearity coupling (a) $\alpha_{\rm self} = 1.1 \times 10^{-6}$, (b) 2.2×10^{-6}, (c) 1.1×10^{-5}

and (d) 2.2×10^{-5}. The results for the local model are very similar. When we compare this picture with Fig. 10 we see the process of vanishing of the ROs are completely different when the dephasing mechanisms is the interface roughness or the electron-electron interaction. In the second case, the effects are the same for any time, then we could not speak about a dephasing time since apparently we only modified the electronic structure and then we are decreasing the resonant coupling between the external ac field and the Bloch bands.

The results that we obtained when we consider together both dephasing effects are more interesting. In Fig. 16 we plot the occupation probability of the state $\psi_1^{(5)}(z)$ as a function of time considering imperfections about one monolayer ($W = 0.03$) for (a) the linear case and considering, together with the imperfections, the electron–electron interaction (b) within the self-consistent model $\alpha_{\text{self}} = 2.2 \times 10^{-6}$ and (c) within the local one $\alpha_{\text{loc}} = 1.1 \times 10^{-1}$. We can clearly see how nonlinearity prevents the dephasing effects introduced by the imperfections allowing the observation of Rabi oscillations during larger coherence times.

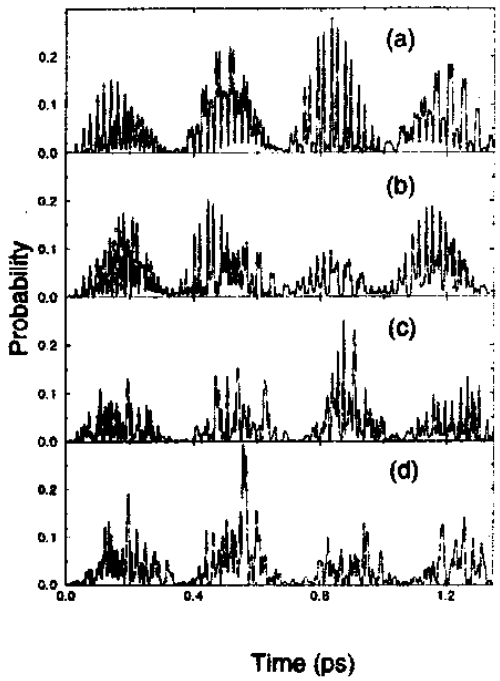

FIG. 15. Probability of finding the electron in the state $\psi_1^{(5)}(z)$ in a perfect SL ($W = 0$) as a function of time when the ac field is tuned to the resonant frequency, $\omega_{\text{ac}} \sim 24\,\text{THz}$, for different values of the nonlinearity coupling (a) $\alpha_{\text{self}} = 5 \times 10^{-5}$, (b) 10^{-4}, (c) 5×10^{-4} and (d) 10^{-3}.

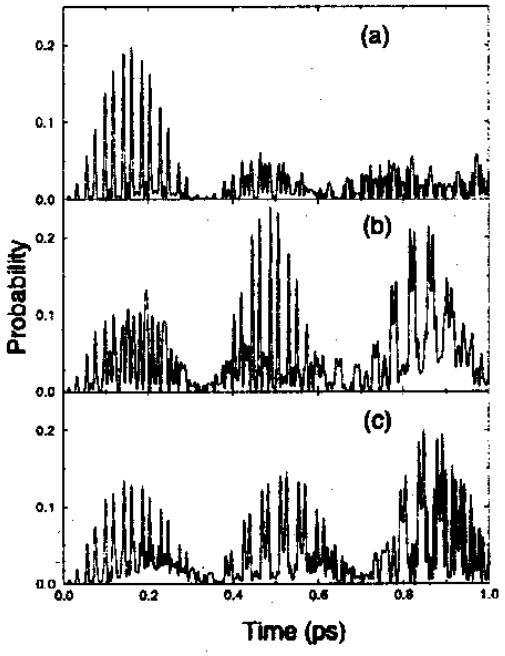

FIG. 16. Probability of finding the electron in the state $\psi_1^{(5)}(z)$ as a function of time for the resonance driving frequency for a SL with imperfections ($W = 0.03$) for (a) the linear case, and modeling the electron–electron interaction with (b) the self-consistent method ($\alpha_{\text{self}} = 2.2 \times 10^{-6}$) and with (c) the local model ($\alpha_{\text{loc}} = 1.1 \times 10^{-1}$).

These theoretical results are completely consistent with recent experiments in transport properties of intentional disordered superlattices with doped and undoped superlattices [85,86], where it is shown that the Coulomb interactions could be the responsible of the suppression of disorder effects leading to quasimetallic behavior at low temperatures when the doping of the samples increases.

7. CONCLUDING REMARKS

One of the main conclusions of this work is to underline the importance of disorder in the transport properties of SLs, in contrast to the general belief that the high quality of actual SLs make the disorder a second order effect. It has to be kept in mind that unintentionally disorder is currently unavoidable, more so when preparing such long SLs (100 periods) as we have considered. In fact, our conclusion is of a quite broader scope, because weak disorder has been usually disregarded as a relevant factor in many other contexts, such as, e.g., studies of optical properties of semiconductors or electronic transport properties in general, to name a few. We note, however, we have restricted the discussion mainly to the single-electron case. As we have shown in the previous section, the dephasing effects of disorder are dramatically reduced when we consider the electron–electron interaction. Other dephasing processes, such as impurity or phonon scattering, have been ignored but could affect the predicted phenomena.

We have been able to firmly connect BOs suppression and dephasing in actual SLs to small deviations from exact flatness at well-barrier interfaces. Specifically, we have shown that an average degree of imperfection of less than one monolayer suffices to explain quantitatively the experimental results reported in [52,59]. Whereas the initially localized state is recovered after time τ_B in the case of perfect ($W = 0$) SLs (regular behavior), any degree of disorder due to imperfections during growth leads to the disappearance of BOs after a few oscillations: The higher the degree of disorder the faster the vanishing of BOs. The very good agreement with previous experiments points out the crucial role of imperfections in the dynamics of actual SLs driven by electric fields. Most importantly, we have been able to define a characteristic scattering time $\tau_{\rm dis}$, *independent* of the electric field, after which BOs cannot be detected, this being a specific prediction of our model that can be checked by experiments. In other words, for the BOs to be observed in actual SLs, the applied electric field must be larger than some critical electric field given by $eF_{\rm dis}L = 2\pi\hbar/\tau_{\rm dis}$. The existence of such a critical field is obviously very important from the viewpoint of practical applications of our results. $F_{\rm dis}$ is directly related to the degree of disorder present in the sample and decreases upon increasing the quality of the sample, i.e., it is an excellent parameter to asses the performance of epitaxial growth techniques.

We have solved the problem of electrons moving in a semiconductor superlattice driven by an ac electric field. We found that the electron can perform ROs under resonant conditions but coherent oscillation vanish due to imperfections during growth: The higher the degree of disorder the faster the vanishing of ROs. Most importantly, we have

been able to define a characteristic scattering time $\tau_{\rm dis}$, *independent* of the electric field, after which ROs cannot be detected, this being a specific prediction of our model that can be checked by experiments. Finally, we have shown that electrons are emitted by *bursts* under resonant conditions, whereas the tunneling probability in vanishingly small out of resonance.

We note, however, that high-frequency operating devices demand higher electric fields. Therefore, for sufficiently high fields, the region where coherent carrier motion takes place, namely $2A_B = \Delta/eF$, is comparable to the SL period L. In such a situation, the in-plane disorder is no longer well described by an ensemble of different quantum wells as we have proposed because the wave packet only would *see* one quantum well. Moreover, we have shown how the dephasing effects of disorder can be overestimated if we do not consider the electron-electron interactions that can reduce dramatically the decoherence effects of the structural imperfections. Our results show that it is possible to enlarge the dephasing times and, consequently, the number of periods of coherence oscillations of electrons in SLs. In semiconductor heterostructures this can be done by increasing the doping or with very intense laser excitation fields. It goes without saying that, to develop new devices for THz science, it is crucial to understand how to control and enlarged the coherence time to exploit the application in ultrafast optical technology: high-speed optical switches, coherent control of excitons, etc. [87,88]. Therefore more theoretical work is needed to investigate the role of imperfections and other dephasing mechanisms like excitonic effects [89,90] in the design of future, shorter period devices.

ACKNOWLEDGMENTS

The authors thank V. Bellani, G. Berman, I. Gómez, R. Gómez-Alcalá, E. Maciá, and A. Sánchez for helpful conversations and work during last years. This work was supported by CAM (Spain) under Project 07N/0034/98.

REFERENCES

[1] L. Esaki and R. Tsu, IBM *J. Res. & Dev.* **14**, 61 (1970).
[2] A. E. Blakeslee and C. F. Aliotta, IBM *J. Res. & Dev.* **14**, 686 (1970).
[3] A. Y. Cho, *Appl. Phys. Lett.* **19**, 467 (1971).
[4] J. M. Woodall, *J. Cryst. Growth* **12**, 32 (1972).
[5] L. Esaki and L. L. Chang, *Phys. Rev. Lett.* **33**, 495 (1974).
[6] D. L. Smith and C. Mailhiot, *Rev. Mod. Phys.* **62**, 173 (1990).
[7] G. Bastard, *Wave mechanics applied to semiconductor heterostructures* (Editions du Physique, 1988).
[8] G. Bastard, *Phys. Rev.* B **24**, 5693 (1981).
[9] S. Adachi, *J. Appl. Phys.* **58**, R1 (1985).
[10] R. M. Feenstra, D. A. Collins, D. Z. -Y. Ting, M. W. Wang, and T. C. McGill, *Phys. Rev. Lett.* **72**, 2749 (1994).
[11] M. Jergel, V. Holý, E. Majková, Š. Luby, R. Senderák, H. J. Stock, D. Menke, U. Kleineberg, and U. Heinzmann, *Physica* B **253**, 28 (1998).
[12] O. E. Raichev, *Phys. Rev.* B **50**, 5462 (1994).
[13] R. J. Turton and M. Jaros, *Appl. Phys. Lett.* **69**, 2891 (1996).

[14] H. Sun, *Phys. Rev.* B **57**, 1674 (1998).
[15] I. Vurgaftman and J. R. Mayer, *Phys. Rev.* B **55**, 4494 (1997).
[16] K. M. Schep and G. E. W. Bauer, *Phys. Rev.* B **56**, 15860 (1997).
[17] U. Penner, H. Rücker, and I. N. Yassievich, *Semicond. Sci. Technol.* **13**, 709 (1998).
[18] M. J. Shaw, *Phys. Rev.* B **58**, 7834 (1998).
[19] H. W. Salemik, O. Albrektsen, and P. Koenraad, *Phys. Rev.* B **45**, 6946 (1992).
[20] S. Gwo, K. -J. Chao, C. K. Shih, K. Sandra, and B. G. Streetman, *Phys. Rev. Lett.* **71**, 1883 (1993).
[21] K. A. Mäder, L. -W. Wang, and A. Zunger, *J. Appl. Phys.* **78**, 6639 (1995).
[22] R. de L. Kronig and W. G. Penney, *Proc. Roy. Soc.* (London) **A130**, 499 (1931).
[23] C. A. Warwick and R. F. Kopf, *Appl. Phys. Lett.* **60**, 386 (1992).
[24] V. I. Belitsky, T. Ruf, J. Spitzer, and M. Cardona, *Phys. Rev.* B **49**, 8263 (1994).
[25] D. F. Nelson, R. C. Miller, C. W. Tu, and S. K. Sputz, *Phys. Rev.* B **36**, 8063 (1987).
[26] M. Proctor, G. Oelgart, H. Rhan, and F. -K. Reinhart, *Appl. Phys. Lett.* **64**, 3154 (1994).
[27] F. Domínguez-Adame, A. Sánchez, and E. Diez, *Phys. Rev.* B **50**, 17736 (1994).
[28] E. Diez, A. Sánchez, and F. Domínguez-Adame, *Sol. Stat. Electron.* **40**, 433 (1996).
[29] E. Diez, F. Domínguez-Adame, E. Maciá, and A. Sánchez, *Phys. Rev.* B **54**, 16792 (1996).
[30] E. Maciá and F. Domínguez-Adame, *Semicond. Sci. Technol.* **11**, 1041 (1996).
[31] B. Jonsson and S. T. Eng, *IEEE J. Quantum Electron.* **26**, 2025 (1990).
[32] T. L. Li and K. J. Kuhn, *J. Comp. Phys.* **110**, 292 (1994).
[33] A. Sánchez, E. Maciá, and F. Domínguez-Adame, *Phys. Rev.* B **49**, 147 (1994).
[34] A. M. Bouchard and M. Luban, *Phys. Rev.* B **52**, 5105 (1995).
[35] J. Feldmann, K. Leo, J. Shah, D. A. B. Miller, J. E. Cuunningham, T. Meier, G. von Plessen, A. Schulze, P. Thomas, and S. Schmitt-Rink, *Phys. Rev.* B **46**, 7252 (1992).
[36] K. Leo, P. Bolivar, F. Brüggemann, R. Schwedler, and K. Köler, *Sol. Stat. Commun.* **84**, 943 (1992).
[37] C. Waschke, H. G. Roskos, R. Schwedler, K. Leo, H. Kurz, and K. Köler, *Phys. Rev. Lett.* **70**, 3319 (1993).
[38] E. Diez, F. Domínguez-Adame, and A. Sánchez, *Microelec. Eng.* **43–44**, 117 (1998).
[39] W. H. Press, B. P. Flannery, S. A. Teukolsky, and W. T. Wetterling, *Numerical Recipes: The Art of Scientific Computing* (Cambridge University Press, New York, 1986) pp. 656-663.
[40] M. Büttiker and R. Landauer, *Phys. Rev. Lett.* **49**, 1739 (1982).
[41] G. Iannaccone and B. Pellegrini, *Phys. Rev.* B **49**, 16548 (1994).
[42] G. Iannaccone, *Phys. Rev.* B **51**, 4727 (1995).
[43] A. Abou-Elnour and K. Schuenemann, *J. Appl. Phys.* **74**, 3273 (1993).
[44] C. M. Weinert and N. Agrawal, *J. Appl. Phys.* **76**, 7947 (1994).
[45] M. Ritze, N. J. M. Horing, and R. Enderlein, *Phys. Rev.* B **47** 10437 (1993).
[46] F. Domínguez-Adame, B. Méndez, and E. Maciá, *Semicond. Sci. Technol.* **9**, 263 (1994).
[47] C. B. Duke, *Tunneling in Solids*, (New York, Academic Press, 1969).
[48] T. B. Boykin, *Phys. Rev.* B **51**, 4289 (1995).
[49] C. Rauch, G. Strasser, K. Unterrainer, W. Boxleitner, E. Gornik and A. Wacker *Phys. Rev. Lett.* **81**, 3495 (1998).
[50] F. Bloch, *Z. Phys.* **52**, 555 (1928).
[51] C. Zener, *Proc. R. Soc.* (London) Ser. A **145**, 523 (1934).

[52] P. Leisching, P. Haring Bolivar, W. Beck, Y. Dhaibi, F. Brüggemann, R. Schwedler, H. Kurtz, K. Leo, and K. Köhler, *Phys. Rev.* B **50**, 14389 (1994).
[53] M. Dignam, J. E. Sipe, and J. Shah, *Phys. Rev.* B **49**, 10502 (1994).
[54] J. Rotvig A. P. Jauho, and H. Smith, *Phys. Rev.* B **54**, 17691 (1996).
[55] G. von Plessen and P. Thomas, *Phys. Rev.* B **45**, 9185 (1992).
[56] M. Sudzius, V. G. Lyssenko, F. Löser, K. Leo, M. Dignam, and K. Köhler, *Phys. Rev.* B **57**, R12693 (1998).
[57] V. G. Lyssenko, G. Valušis, F. Löser, T. Hasche, K. Leo, M. Dignam, and K. Köhler, *Phys. Rev. Lett.* **79**, 301 (1997).
[58] K. Leo, *Semicond. Sci. Technol.* **13**, 249 (1998).
[59] G. von Plessen, T. Meier, J. Feldmann, E. O. Göbel, P. Thomas, K. W. Goosen, J. M. Kuo, and R. F. Kopf, *Phys. Rev.* B **49**, 14058 (1994).
[60] A. M. Bouchard and M. Luban, *Phys. Rev.* B **47**, 6815 (1993).
[61] J. P. Reynolds and M. Luban, *Phys. Rev.* B **54**, R14301 (1996).
[62] T. Dekorsy, P. Leisching, K. Köhler, and H. Kurz, *Phys. Rev.* B **50**, 8106 (1994).
[63] C. Cohen-Tannoudji, B. Diu, and F. Laloë, *Quantum Mechanics* (Wiley, New York, 1977).
[64] I. I. Rabi, *Phys. Rev.* **51**, 652 (1937).
[65] I. I. Rabi, S. Milliman, P. Kusch, and J. R. Zacharias, *Phys. Rev.* **55**, 526 (1939).
[66] H. C. Torrey, *Phys. Rev.* **76**, 1059 (1949).
[67] S. T. Cundiff, A. Knorr, J. Feldmann, S. W. Koch, E. O. Göbel, H. Nickel, *Phys. Rev. Lett.* **73**, 1178 (1994).
[68] G. B. Hocker and C. L. Tang, *Phys. Rev. Lett.* **21**, 591 (1968).
[69] T. Martin and G. P. Berman, *Phys. Lett.* A **196**, 65 (1994).
[70] C. A. Stafford and N. S. Wingreen, *Phys. Rev. Lett.* **76**, 1916 (1996).
[71] X. -G. Zhao, G. A. Georgakis, and Q. Niu, *Phys. Rev.* B **54**, R5235 (1996).
[72] E. Diez, R. Gómez-Alcalá, F. Domínguez-Adame, A. Sánchez, and G. P. Berman, *Phys. Lett.* A **240**, 109 (1998).
[73] K. Nakamura, A. Shimizu, M. Koshiba, K. Hayata, *IEEE J. Quantum Electron.* **25**, 889 (1989).
[74] H. Drexler, J. S. Scott, S. J. Allen, K. L. Campman, and A. C. Gossard, *Appl. Phys. Lett.* **67**, 2816 (1995).
[75] C. Presilla, G. Jona-Lasinio, and F. Capasso, *Phys. Rev.* B **43**, 5200 (1991).
[76] G. Jona-Lasinio, C. Presilla, and F. Capasso, Phys. Rev. Lett. **68**, 2269 (1992).
[77] G. Jona-Lasinio, C. Presilla, and J. Sjöstrand, Annals of Physics **240**, 1 (1995).
[78] N. G. Sun and G. P. Tsironis, *Phys. Rev.* B **51**, 11221 (1995).
[79] E. Diez, F. Domínguez-Adame, A. Sánchez *Phys. Lett.* A **198**, 403 (1996).
[80] R. Knapp, G. Papanicolaou, and B. White, *J. Stat. Phys.* **63**, 567 (1991).
[81] E. Diez, A. Sánchez, and F. Domínguez-Adame, *Phys. Lett.* A **215**, 103 (1996).
[82] E. Cota and S. E. Ulloa, *Phys. Rev.* B **51**, 10875 (1995).
[83] M. S. Sherwin, K. Craig, B. Galdrikian, J. Heyman, A. Markelz, K. Campman, S. Fafard, P. F. Hopkins, and A. Gossard, *Physica* D **83**, 229 (1995).
[84] J. Devis, E. Diez and V. Bellani, *Phys. Lett.* A (in press).
[85] G. Richter, W. Stolz, P. Thomas, S. W. Kock, K. Maschke, and I. P. Zvyagin, *Superlattices and Microstructures* **22**, 475 (1997).
[86] V. Bellani, E. Diez, R. Hey, L. Toni, L. Tarricone, G. B. Parravicini, F. Domínguez-Adame, and R. Gómez-Alcalá, *Phys. Rev. Lett.* **82**, 2159 (1999).
[87] D. S. Citrin, *Phys. Rev. Lett.* **77**, 4596 (1996).
[88] D. S. Citrin, *Appl. Phys. Lett.* **70**, 1189

(1997).
[89] D. M. Whittaker, *Eurohys. Lett.* **31**, 55 (1995).
[90] G. Valušis, V. G. Lyssenko, D. Klatt, F. Löser, K. H. Pantke, K. Leo and K. Köhler *Proceedings of the 23rd Int. Con. on The Physics of Semiconductors, 1996*, Ed. M. Scheffler and R. Zimmermann, pp. 1783-1787, World Scientific (1996).